Journal of
Microscopy

Journal of Microscopy, Vol. 00, Issue 0 2017, pp. 1–13
Received 17 August 2016; accepted 23 February 2017

doi: 10.1111/jmi.12560

SEM-microphotogrammetry, a new take on an old method for generating high-resolution 3D models from SEM images

A.D. BALL*, P.A. JOB† & A.E.L. WALKER*
*Imaging and Analysis Centre, Core Research Laboratories, The Natural History Museum, London, U.K.
†Centre for Ecology and Conservation, College of Life and Environmental Sciences, University of Exeter, Exeter, U.K.

Key words. Confocal microscopy, 3D printing, micro-CT, photogrammetry, SEM.

Summary

The method we present here uses a scanning electron microscope programmed *via* macros to automatically capture dozens of images at suitable angles to generate accurate, detailed three-dimensional (3D) surface models with micron-scale resolution. We demonstrate that it is possible to use these Scanning Electron Microscope (SEM) images in conjunction with commercially available software originally developed for photogrammetry reconstructions from Digital Single Lens Reflex (DSLR) cameras and to reconstruct 3D models of the specimen. These 3D models can then be exported as polygon meshes and eventually 3D printed.

This technique offers the potential to obtain data suitable to reconstruct very tiny features (e.g. diatoms, butterfly scales and mineral fabrics) at nanometre resolution. Ultimately, we foresee this as being a useful tool for better understanding spatial relationships at very high resolution. However, our motivation is also to use it to produce 3D models to be used in public outreach events and exhibitions, especially for the blind or partially sighted.

Introduction

There are five common techniques to nondestructively acquire three-dimensional (3D) data of microscopic and macroscopic samples:

(1) **Micro-CT** which uses X-rays to image the specimen and provides a dataset in the form of a 3D volume, is very rapid, can be very high resolution (particularly through the use of synchrotron X-ray microcomputed tomography) and is insensitive to sample surface reflectivity. 3D volumes can be converted easily to 3D surface models.

(2) **Confocal microscopy** which creates a 3D volume dataset using scanning laser-induced fluorescence, but requires the sample to be transparent for best results in generating a 3D volume dataset. Reflection mode confocal microscopy can also be used to acquire a 3D dataset of the sample surface. Both techniques can easily yield 3D surface models.

(3) **Surface scanning** using either lasers or structured light is comparatively rapid, provides 3D point cloud or polygon mesh data, but has limited resolution (down to a few hundreds of microns) and can be very sensitive to surface reflectivity, transparency or opacity changes in the specimen. This technique only yields surface models.

(4) **Z-stacking** is a technique used to create an iso-surface based on computed focal planes. The technique is light microscopy-based and is thus sensitive to sample type and cannot reconstruct reflective or transparent surfaces. Steep-sided or undercut surfaces are not effectively modelled, thus the models are 3D surfaces, but only of the surface visible to the imaging system.

(5) **Photogrammetry** uses a reconstruction based on large numbers of photographs taken from different orientations to create point cloud or 3D polygon mesh data. Since this is a photographic technique, it is sensitive to surface lighting, transparency and reflectivity of the sample and to depth of field in the images. The data acquired produce 3D surface models of the sample. The resolution is lower compared to the other techniques described. However, the equipment required is relatively simple, making it extremely cost-effective.

Where the emphasis is on high-resolution data acquisition (micron- and submicron), the choices in nondestructive techniques are typically limited to micro-CT and confocal microscopy, since both can yield submicron resolution. Laboratory-based micro-CT systems can now yield submicron data (nano-CT) which makes these systems a more accessible alternative to synchrotron tomography for many applications.

Correspondence to: A.D. Ball, Imaging and Analysis Centre, Core Research Laboratories, The Natural History Museum, London SW7 5BD, U.K. Tel: 0207 942 5263; e-mail: a.ball@nhm.ac.uk

© 2017 The Authors
Journal of Microscopy © 2017 Royal Microscopical Society

To these techniques, **scanning electron microscopy** (**SEM**) can also be added, since reconstruction of 3D data from SEM has been possible since the 1970s.

SEM overcomes many of the traditional limitations of light microscopy, offering excellent depth of field, high resolution and good sample sensitivity across a wide range of materials. Reconstructing 3D surfaces using SEM is not new and there are several programs and commercialized methods which allow 3D data to be obtained from samples using SEM data. However, these methods typically fall into two categories:

(1) those that obtain 3D information from a tilt series across a single axis through analysis of a stereo pair or triplet image series (e.g. Alicona's MeX software – Alicona Imaging GmbH, Austria)
(2) those that obtain data through acquiring information with an angular offset using a four quadrant backscattered electron (BSE) detector (e.g. SEM topography – Point Electronic GmBH, Saale Germany).

Although these methods can be effective for analysing features with limited topography (Kearsley *et al.*, 2007), they cannot accurately model complex 3D objects. For example, steep-sided features and overhangs are poorly rendered since the images used for analysis are obtained from a very limited series of viewpoints.

SEM-hosted structure from motion (SfM) photogrammetry, the technique described here, can provide submicron resolution on topographically complex objects. However, SfM 3D photogrammetry reconstruction techniques applied to SEM datasets have previously relied upon complex workflows and custom-written code and demonstrated only limited ability to recreate complex 3D structures (e.g. Cornille *et al.*, 2003; Tafti *et al.*, 2015). Eulitz & Reiss (2015) describe a broadly similar approach to that utilized in this study, but their approach used manual control of the SEM and utilized just 40 images for their reconstruction of a single model of a rabbit glomerulus. The approach demonstrated here uses automated macros to run the SEM for stage movement and image capture and utilizes commercially available software following a workflow very similar to that used for conventional SfM photogrammetry.

The use of SfM photogrammetry to yield 3D reconstructions by combining dozens to hundreds of photographic images of a subject taken from different viewpoints is becoming increasingly common, particularly as a mechanism to acquire 3D data in palaeontology and cultural heritage research (Micheletti *et al.*, 2015) and even for entomological samples (Nguyen *et al.*, 2014). The approach demonstrated here draws from the methods more commonly used in palaeontology, where the use of SfM photogrammetry is well established (e.g. Falkingham, 2012; Mallison & Wings, 2014; Sutton *et al.*, 2014; Fahlke & Autentrieth, 2016) and also widely used in the film and video game industries.

SfM photogrammetry

Structure from motion photogrammetry relies on computing the 3D form of the object or feature of interest from a series of overlapping images taken from different viewpoints. These can be achieved either by moving the camera around the object, or rotating the object within the field of view. This is similar to stereoscopic photogrammetry, but does not rely on the relative position between the object of interest and the camera being known. Instead, these are calculated through automatic identification of matching features across a series of overlapping images. This allows the software to calculate the camera positions relative to the object as well as the 3D geometry of the scene or sample (Snavely *et al.*, 2008). The term 'structure from motion' refers to the motion of the sensor relative to the scene being recorded. Micheletti *et al.* (2015) and Westoby *et al.* (2012) describe different approaches to the use of SfM for geological applications, both of which provide a good introduction to the historical development and principles underlying SfM.

Here, we describe an automated method to obtain data suitable for 3D reconstruction by SfM photogrammetry using a wide range of samples and several different scanning electron microscopes. We also provide a limited review of a number of programs available to reconstruct photogrammetry data and comment on their suitability to reconstruct images from SEM.

Methods

Three SEMs were used for this study: a Zeiss Ultra Plus, a (Zeiss) LEO 1455VP and an FEI Quanta 650 FEG. The SEM, its stage and image capture system were controlled through easily modified, programmable macro languages. The Zeiss instruments have the macro control built in as part of their base functionality. The FEI Quanta was programmed using software supplied by the manufacturer to support this project.

All samples were mounted on standard 12 mm aluminium pin stubs and coated with 20–60 nm of gold palladium using a Cressington HR208 sputter coater utilizing a quartz crystal monitor to control the coating thickness. One to three successive 20 nm coats were applied using the planetary tilt and rotate stage in the sputter coater to ensure that the coatings were applied continuously over the sample.

SEM was carried out at 15–20 kV on the LEO 1455VP and FEI Quanta and at 5–7 kV on the Zeiss Ultra Plus. Spot size, aperture settings and working distance were chosen to maximize focal working depth. (See results for further information.)

Each image needs to be acquired with the sample correctly centred to ensure that sufficient overlap with adjacent images can be identified by the reconstruction software. The macros written to control the stage require that the sample height,

© 2017 The Authors

centre of rotation and tilt centre be correctly calibrated. These calibration steps differed between the Zeiss and FEI instruments, but achieve the same goal.

The image acquisition macros were used to acquire the following image series:

(1) At 0° tilt, four images were acquired at 90° stage rotation intervals.
(2) For tilted samples, 36 or 72 images were acquired at 5 or 10° stage rotation intervals (36 images were usually adequate, but since this process was automated, 72 images were generally acquired at each tilt angle).

The tilt sequence typically acquired images at four or five different tilt angles. On the LEO, these were acquired at 10°, 30°, 50°, 70°and 90°. The Quanta and Ultra Plus were unable to tilt the stage beyond 70°, so the 90° tilt increment was omitted and images were acquired at 15, 30, 45 and 60 or 70° tilt angles (Fig. 1). This allowed the acquisition of a series of images which covered the sample surface with an appropriate level of overlap.

Photogrammetry reconstruction of the data used Agisoft PhotoScan Professional (version no. 1.1.6 http://www.agisoft.com/). The workflow typically involved an initial image alignment and test using the lowest possible quality settings to rapidly assess the accuracy of the computed

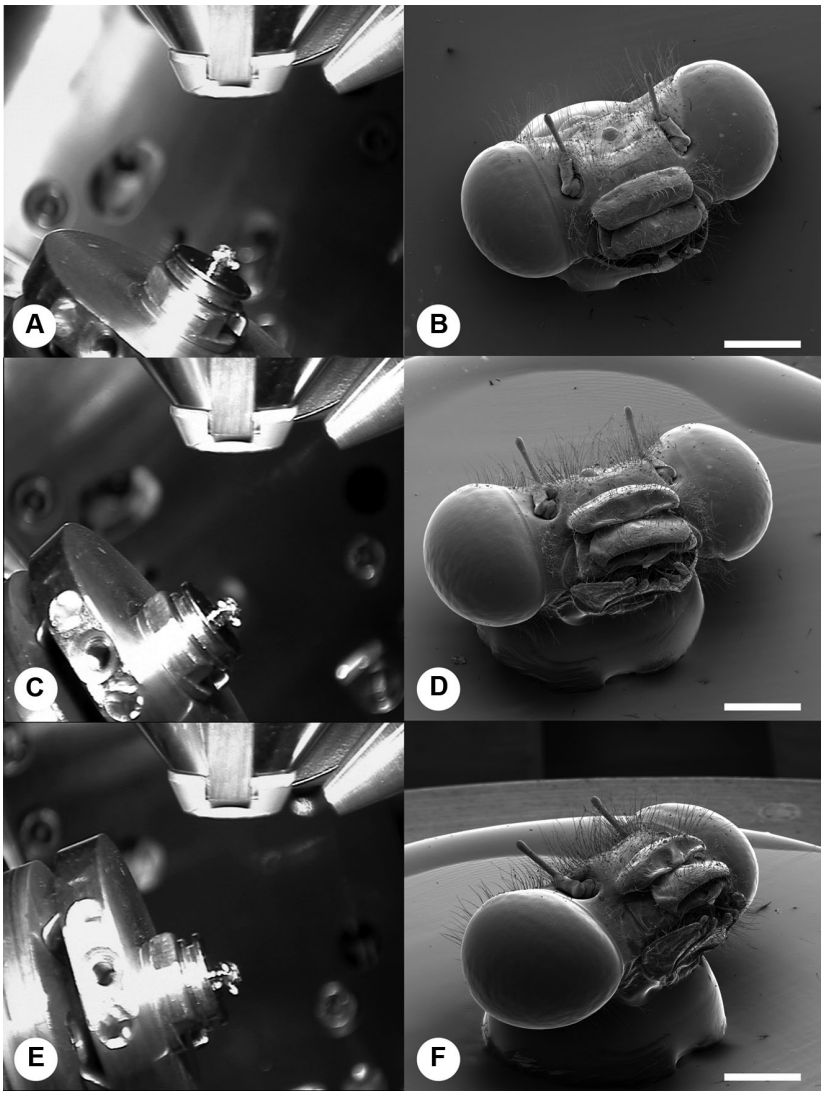

Fig. 1. (A) Internal camera view of the microscope chamber showing mounted specimen tilted at 15°, **(B)** corresponding image of damselfly head, **(C)** SEM stage tilted to 45°, **(D)** corresponding SEM image, **(E)** SEM stage tilted to 70° and **(F)** corresponding SEM image. Note that as the tilt angle increases, details of the lateral view of the specimen become visible. This is essential for the reconstruction process since it reveals details below overhanging features. Note the resin beads used to raise the specimen above the surface of the stub and thus increase the amount of detail captured on the lower surface of the specimen. Scale bars 500 μm.

© 2017 The Authors

camera positions (this typically takes 15–20 min). If these were correct, then the software was run in 'high quality' mode using the batch operation option, usually overnight. If the camera positions were incorrectly computed, the alignment procedure was rerun to correctly align the missing cameras. The methodology followed for the use of Photoscan was substantially similar to that described in detail in Mallison & Wings (2014).

Successfully reconstructed datasets were exported as .stl mesh files and then edited in Autodesk's Meshmixer software package (http://www.meshmixer.com/) to remove any holes, repair defects in the mesh and finally to create a model suitable for 3D printing. This process is too complex to outline in this paper, but is widely documented in Autodesk's online tutorials (https://www.youtube.com/playlist?list = PLu8TYSQ5jCFjdQBHsLoybhdKXOTmpTRlb).

The 3D printed models were initially produced using a Formlabs Form 1+ printer (http://formlabs.com/). Many of the models were too complex to be printed and were downsampled (simplified) using Meshlab (http://meshlab.sourceforge.net/). This requirement was found to be a limitation of the Formlabs printer which could not handle a file larger than 25 MB on the hardware used for the project, other printer/hardware combinations should be capable of reproducing higher resolution meshes.

Results

A number of different samples were imaged and modelled including insect heads (Fig. 2), snail shells, a diatom, schistosomes, a micrometeorite impact crater, sections of butterfly wing and finally a single, isolated, butterfly wing scale (Fig. 3). These samples were chosen to test the technique at a range of magnifications (from ~ 20x to 1000x) and sample geometries (from spherical samples to flat specimens). In general, the technique was more successful with objects which are approximately spherical (hence,the technique worked well for insect heads and shells). Objects which were flattened (diatom, impact crater and butterfly wing) proved more problematic to reconstruct (Figs. 3**B, D, E**) since it was more difficult to obtain the high tilt angle images needed to distinguish between the specimen and the background. This was resolved with the butterfly scale by mounting it onto a TEM grid, but the diatom, which was mounted directly onto mica attached to the stub, was not well differentiated from the background and the impact crater was reconstructed as a continuous extension of the layer from which it was extruded.

Sample mounting and coating

The best results were obtained from samples which were raised slightly above the surface of the stub, this allowed the 3D re-

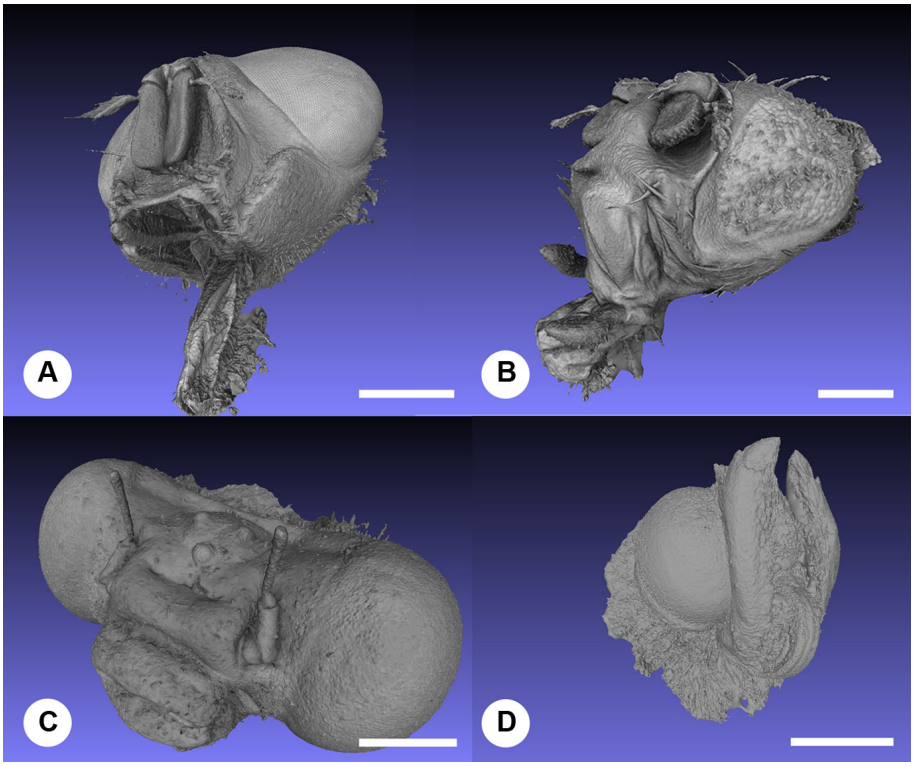

Fig. 2. 3D models reconstructed from SEM photogrammetry data. **(A)** Blowfly head, **(B)** fruitfly head, **(C)** damselfly head **and (D)** butterfly head. These images are screenshots of stereolithography file meshes displayed in Meshlab. Scale bars 500 μm.

© 2017 The Authors

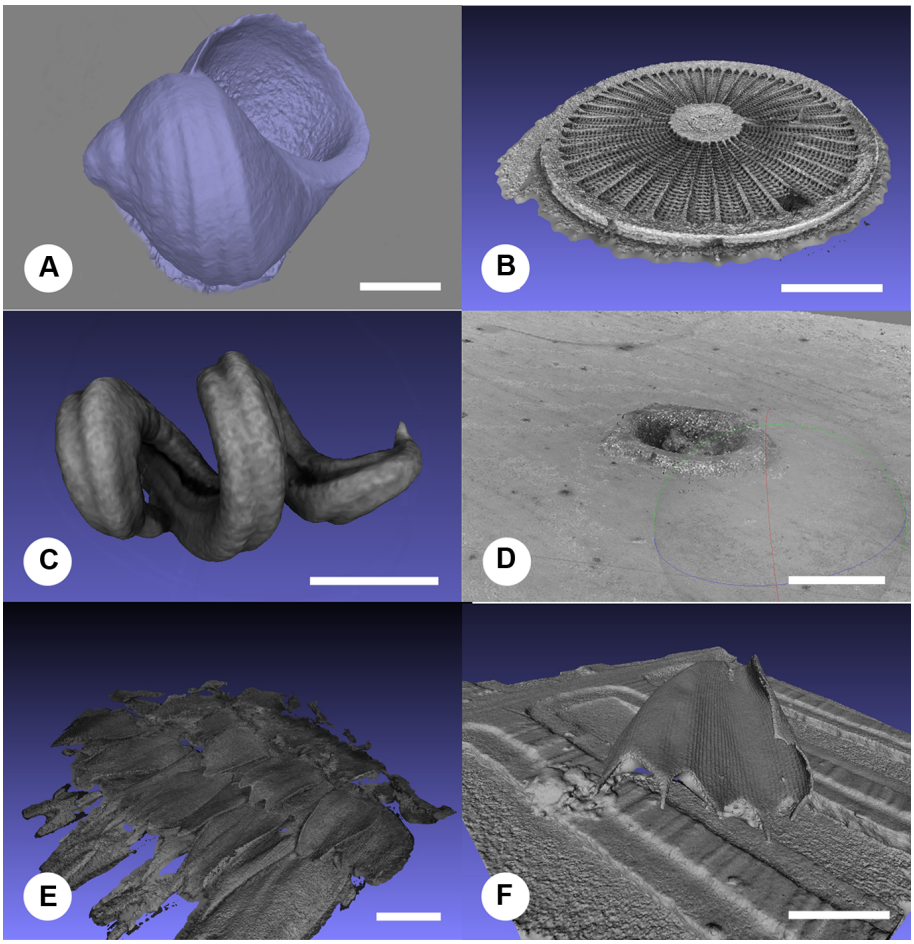

Fig. 3. 3D models reconstructed through SEM photogrammetry. (**A**) Littorinid snail shell, (**B**) diatom, (**C**) schistosomes (the male is wrapped around the female), (**D**) synthetic micrometeorite impact crater into aluminium foil, (**E**) section of butterfly wing showing scales and (**F**) single isolated butterfly scale on a TEM grid. These images are screenshots of stereolithography file meshes displayed in Meshlab. Scale bars: (**A**) 250 μm, (**B**) 100 μm, (**C**) 2 μm (**D**) 60 μm, (**E**) 200 μm and (**F**) 100 μm.

construction software to better separate the specimen from the stub surface. This was achieved by casting small hemispheres (~3 mm diameter) in Araldite resin, gluing these to the stubs and then attaching the specimens to the araldite hemispheres (Figs. 1**B, D, F**). Most samples were coated in three successive layers of gold-palladium, amounting to a total maximum thickness of 60 nm. This rather heavy coating was necessary to prevent charging during the automated imaging process. Early experiments used uncoated samples in variable pressure mode on the LEO 1455. This was successful, but acquiring each image took approximately 7 min to obtain good signal to noise ratios at the extended working distances required to deliver the necessary depth of field. This made the acquisition process too long to be feasible. Coating the samples allowed for faster acquisition (~ 2 min per frame) and less 'noisy' images. This in turn generated better final reconstructions.

Stage calibration

For successful photogrammetry data acquisition, the software needs to match as much of one image to the next as possible, thus, ideally, the specimen needs to be correctly centred in each image. This requires the specimen height, compucentric or eucentric tilt (which ensures that the specimen remains within the centre of the field of view when the stage is tilted) to be calibrated. As the sample rotates, the microscope needs either to be capable of compucentric rotation (where the software calculates the X and Y stage offsets for each movement in the rotational axis to ensure that the specimen remains centred in the field of view as it rotates) – which requires further calibration, or these calculations need to be done manually and the stage X/Y offset positions entered for each rotational stage movement and subsequent image capture step. For the Zeiss instruments used, an initial set-up routine is required for the stage centre to be accurately calibrated. The specimen was

© 2017 The Authors

then tested at different tilt angles to ensure that the compucentric tilt and rotate function were also working correctly. To verify these calibrations, a short macro was written to acquire a series of images at four 90° offsets.

For the FEI Quanta, the standard compucentric rotational calibration procedure was adequate at low tilt angles (up to 20°), but at higher tilt angles, the X/Y stage offsets had to be manually calculated and entered into the software. To aid this, a simple Microsoft Excel macro was written to generate the required stage coordinates which were entered into the FEI macro language.

Image set-up

Other factors found to be important in data acquisition were sample 'illumination' and depth of field. To model the sample in 3D, the reconstruction software performed best if the whole sample was focussed and evenly 'illuminated' with minimal shadowing. 'Illumination' in this case refers to the evenness of the brightness and contrast and lack of shadows in the final image. Initial comparisons between the secondary electron detector (SE) and the solid-state BSE detector showed that the strong directionality of the signal from the SE detector led to shadowing of the sample in the final image (Fig. 4**A**). This did not lead to effective reconstruction of the final 3D model. It was found that the lack of preferential 'illumination' from the BSE detector, which gave an even, rather 'flat' looking image compared to the SE detector (Fig. 4**B**), yielded a better reconstruction. This was especially apparent in reconstructions of highly topographical structures. Photogrammetry software requires very even illumination of the subject for best results and the BSE images lack areas of strong shadow and contrast and met these criteria better than the SE images.

The depth of field in the image could be maximized through two mechanisms: working distance and aperture settings. In an SEM, the use of a long working distance combined with a narrow aperture will deliver an image with much greater depth of field than could be obtained with a light microscope. The three SEMs each utilized different strategies to maximize the depth of field:

(1) For the FEI Quanta, the aperture and spot sizes were chosen to give the best compromise between signal to noise ratio and depth of field.
(2) In the LEO, extended working distances were used to provide the required depth of field (Figs. 4**C, D**). Since the LEO in our laboratory normally operates exclusively in variable pressure mode and the variable aperture strip is withdrawn under these conditions, this was the only mechanism available to provide greater depth of field (other than reconfiguring the microscope).
(3) For the Zeiss Ultra Plus, using a small aperture resulted in a signal level too low for the BSE detector to work effectively. Larger apertures did not deliver adequate depth of field. However, the SEM has a 'high current mode' which allows access to a lens setting which artificially increases the depth of field in the final image; this is independent of the aperture selected. The result is that the microscope can simultaneously maximize the signal available, by use of a large aperture and still provide an extended depth of field in the image (Figs. 4**E, F**).

Acquisition strategy

The objective is to acquire a series of images which capture the specimen from as many different angles as possible. If the specimen can be imagined as a 'planet', the camera needs to take a series of photos to form strips of images which overlap to capture the whole of the planet surface. To do this, the camera needs to 'orbit' at a number of different latitudes and at the poles for a complete map of the 'planet' (Fig. 5**A**). For SEM photogrammetry, only a single hemisphere was imaged due to the tilt limitations of the stages used in the study, but this was sufficient to produce models of all the samples.

Some experimentation was carried out to establish the optimum number of rotational images to acquire in each 'orbit'. Theoretically, the number of images required can be obtained by using the SEM working distance as the radius of a circle with the specimen at its centre (Fig. 5**B**). From this, the circumference can be calculated and divided by the width of each image to arrive at the minimum number of frames required to capture every part of the specimen with no overlap. A larger number of images (allowing for the required overlap) can then be captured.

For example, at a working distance of 22 mm, the effective circumference of the circle surrounding the sample is approximately 138 mm. If 36 images are taken of the sample, the width of each image would need to be at least 3.85 mm to cover this circumference. This value would then define either the minimum magnification required to achieve this value, or the minimum number of rotational images to obtain a desired overlap between one image and the next.

Trials were made with 72 or 36 images (5° or 10° rotational step between images), but there appeared to be a little change in the model result despite the fact that 72 images would provide more overlap. Since the acquisition sequence was automated, there was no 'human cost' in taking more images, so in most cases 72 images were collected, although some of the data presented in the results are based upon 36 images.

In most cases, four or five different tilt angles were collected (Fig. 5**C**). Failing to collect enough tilt angles, especially at high tilt angles, led to a failure in the model to accurately reflect the topology of the sample (Fig. 5**D**).

The biggest limitation to image capture was the relatively poor resolution of the standard SEM frame store (~ 3 k × 2 k for the Zeiss instruments and 6 k × 4 k for the FEI Quanta). The relatively low resolution in the images means that fine features

© 2017 The Authors

(antennae, fine surface detail, etc.) are not adequately sampled and thus not reconstructed (Fig. 5E). Although this resolution is broadly similar to that of a contemporary 'prosumer' dSLR with a 20 megapixel image sensor, dedicated accessory frame stores can capture up to 32 k × 32 k in each image.

To try to overcome the frame store size limitation, and to increase the resolution in the final model, another trial was attempted using the Zeiss Ultra Plus, with the aim of maximizing the number of pixels captured across the surface of the sample. In this trial, the revised macro captured a series of images at varying tilt angles (with no sample rotation), then returned to the initial tilt angle, rotated the stage and started a new tilt sequence (Fig. 5F). This approach aimed to achieve higher magnifications in the initial image, because the automated combination of tilt and rotate captured more image overlap. Although this scheme did allow for impressive reproductions of small areas of the surface, the stage proved incapable of making the complex movements in X, Y tilt and rotate required for this strategy. (See later comments on stage performance.)

Acquisition times were typically 40–120 s per frame, although acquisitions as low as 3 s proved successful with some specimens. A rotational dataset requires approximately 2 h data collection, with four tilt angles taking the total acquisition time to about 8 h. Higher resolution image capture might take as long as 8 min per frame, leading to total acquisition times of approximately 20 h. However, it was found that it was possible to remove the sample and reposition it between image capture runs allowing for automated data collection over 2–3 nights.

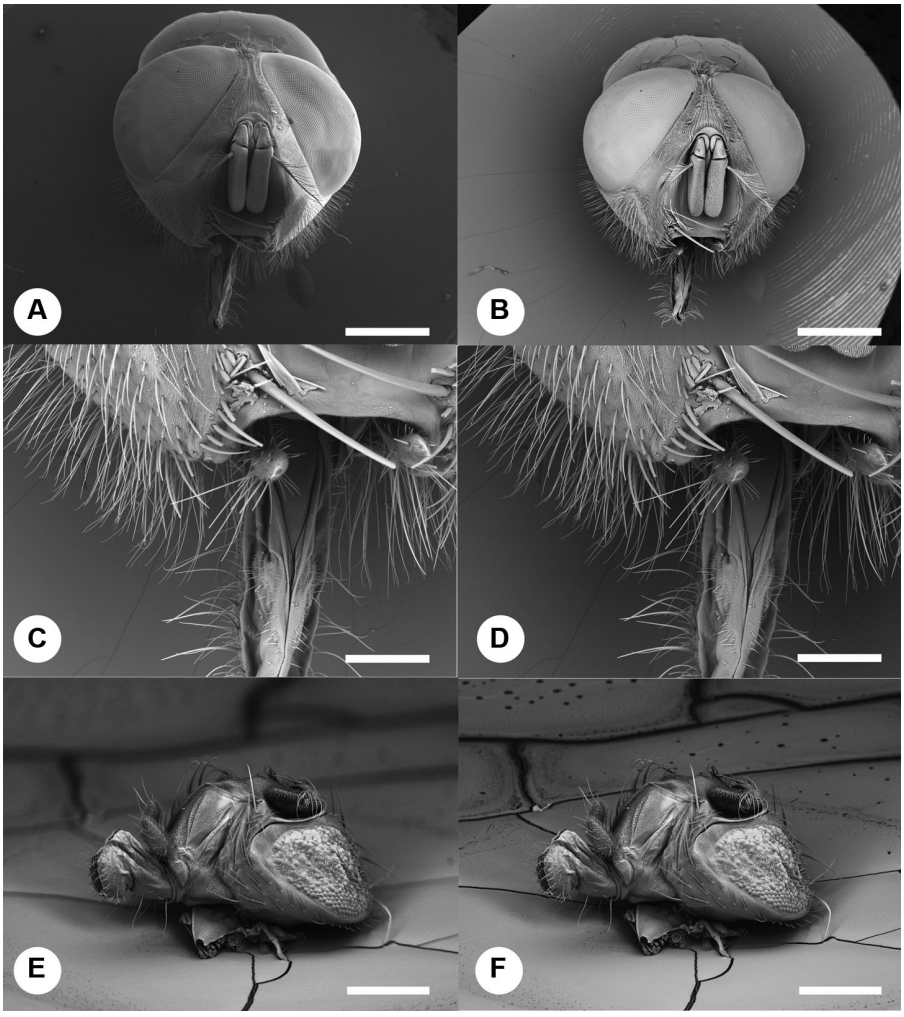

Fig. 4. Microscope set up and its effect on illumination and depth of field. (**A**) Secondary electron image shows strong directional illumination, (**B**) backscattered electron image shows a very even illumination of the specimen, with little shadowing, (**C**) shallow depth of field obtained at short working distance, (**D**) greater depth of field is obtained at longer working distance at the expense of some loss of signal [images (**A–D**) taken using the LEO 1455], (**E**) shallow depth of field in the Zeiss Ultra Plus is compensated for by the use of high current mode, (**F**) which increases the depth of field considerably. Scale bars: (**A**), (**B**) 500 μm, (**C**), (**D**) 250 μm and (**E**), (**F**) 500 μm.

© 2017 The Authors

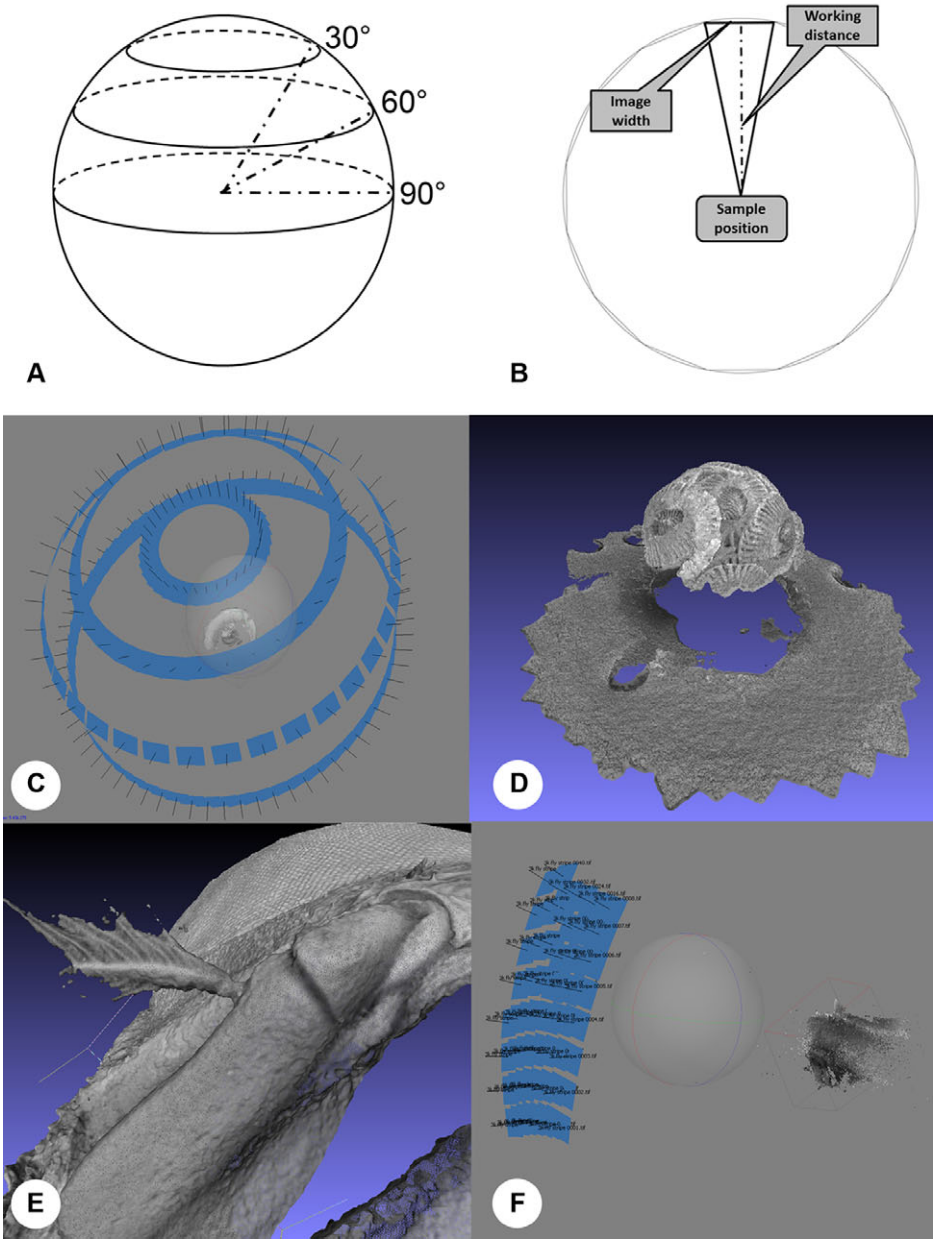

Fig. 5. Acquisition strategies. (A) Diagram illustrating the effective viewpoint of three different tilt angles showing how the circumference of the spherical cap increases with tilt angle, requiring more images to achieve the same level of image overlap, (**B**) the number of images required is determined by calculating the circumference of a circle defined by the working distance (radius), the magnification required to capture the whole specimen in the field of view defines the image width in microns, (**C**) simulated camera positions from images acquired at four different tilt angles show that the data closely match the modelling in (**A**), (**D**) the effect of acquiring insufficient high tilt angle data – the specimen lacks information around its base, (**E**) lack of fine captured detail as a result of insufficient pixel coverage of the smaller features in the specimen and (**F**) simulated camera positions from alternative image capture strategy where the images are captured in vertical stripes at different tilt angles, before returning the stage to zero tilt and then rotating the specimen.

Stage reproducibility and accuracy

Over the trials conducted, it was quite clear that a major limitation of the method was not the macros employed, nor the resolution of the frame store, but the ability of the stage to return to fixed positions after long sequences of repeated small stage movements. Over time, the backlash accumulated in the stage allowed the specimen to drift towards the edge of, or

© 2017 The Authors

entirely out of, the field of view. This proved to be a factor which ultimately limited the maximum magnification which could be employed during the trials. Employing backlash correction in the software did not overcome this problem and it was determined that the 'standard' microscope stages utilized simply did not have sufficient repeatable accuracy for such a demanding task. Imaging was thus generally carried out at relatively low magnifications. However, tests were carried out on some samples at high magnifications making manual corrections to recentre the specimen (Figs. 3**B, D, E, F**) to test whether the technique was viable at high magnifications. To obtain the reconstruction in Figure 3**(B)** (obtained using the FEI Quanta 650) involved considerable human intervention to correct stage positioning errors.

Reconstruction of the data

Photogrammetry is an increasingly popular technique to reproduce objects in 3D and is widely used as a tool for image capture as part of 3D modelling and 3D printing workflows. As a result, there are a variety of free, online and commercial software packages available. During this study, a number of different software packages were evaluated to determine their suitability for reconstructing SEM-derived data.

Four programs were tested: **Visual SFM** (http://ccwu.me/vsfm/), **Insight3D** (http://insight3d.sourceforge.net/), **123D Catch** (http://www.123dapp.com/catch) and **Agisoft Photoscan Professional** (http://www.agisoft.com/). Of these packages, Visual SFM, Insight3D and 123D Catch are free to use, whereas Photoscan is a commercial package which can be tested for free (although the data cannot be saved). Of the free packages, 123D Catch is the easiest to use, Visual SFM delivered the best results and Insight3D appears to be the most limited. However, since Photoscan delivered the best overall performance, it was the focus of all our testing after the initial evaluation had been completed.

Under normal use cases, Photoscan makes use of the 'EXIF' (**EX**changeable **I**mage **F**ile) data standard which is embedded into digital images derived from modern digital cameras. These data describe the camera sensor (size and number of pixels) and the lens characteristics (focal working distance and focus settings) and from these, the software can calculate the distance between the camera and the object being photographed. Overlap between adjacent images allows pixels to be matched and the camera position relative to the object to be calculated. Simulated camera positions are displayed in software (Figs. 5**C, F**) to allow for misaligned cameras to be identified and realigned. The camera data can also be manually entered into the program. However, SEM images have no such corresponding information, do not have sensors in the same sense as digital camera and no comparable focal length. Nevertheless, even without this information, it proved possible for the software to generate a robust reconstruction with good simulated camera positions. The end result could be exported as a point cloud or mesh dataset and was thus compatible with 3D modelling and data analysis packages and even allowed the data to be 3D printed.

Reconstruction times were dependent on the density of the point cloud required and the resolution of the mesh computed. Typically, a reconstruction of about 15 min on a dual processor 3.2 GHz Intel Zeon PC with 32 GB of RAM proved adequate to generate a low-resolution model to assess the quality of the data. Photoscan has the facility to batch process the entire dataset, so most high-resolution reconstructions were carried out overnight. Tests on computers with more RAM showed that significant time savings can be made if this option is available.

Model output

All of the insect heads were rendered effectively at the gross scale (Fig. 2), but inspection of the model at higher magnification showed that surface hairs, setae and complex features (antennae and fly mouthparts) were not accurately captured (Fig. 5**E**). However, the simple, rod-like, antennae of the damselfly were correctly modelled (Fig. 2**C**). Inspection of the data suggests that modelling of the relatively fine setae and fly antennae was inaccurate because the image resolution was too low to capture these features in sufficient detail for the software to identify individual setae across successive images. The damselfly antennae, however, because they were larger, occupied more pixels in the source images and were thus correctly reconstructed. It is worth noting that 3D modelling of 'hair' is a highly computationally complex problem (see, e.g. Beeler *et al.,* 2012 for a discussion and methods for modelling of human hair from photogrammetry data) which is beyond the capability of this software. Some larger setae were successfully reconstructed, but the very fine setae could not be modelled. As a result, in the 3D models and subsequent prints, surfaces with very fine-scale structures were not accurately reproduced.

Features which were flatter and smaller – for example the diatom (Fig. 3**B**), micrometeorite impact crater (Fig. 3**D**) and section of butterfly wing (Fig. 3**E**) were less effectively modelled since it was not possible to capture the very high tilt angle images of the sample which are necessary to separate the fine-scale edge detail from the surface upon which they were lying. For example, the model of the impact crater (Fig. 3**D**) does not entirely reflect the complexity of the rolled edges of the uplifted foil seen in the SEM (Fig. 6**B**). The diatom model is also missing the upright diatoms embedded within it (compare the model result in Fig. 3**B** with one of the SEM source images in Fig. 6**A**) and the repeating structures were not accurately modelled – most likely due to a lack of resolution in the source images (despite these being 6 k × 4 k images). However, the isolated butterfly scale (Fig. 3**F**) was extremely faithfully reproduced; including the fine-scale ridges which are only a few microns wide (see SEM source images Fig. 6**C**). This may be because the textured background (a TEM grid) helped the software

© 2017 The Authors

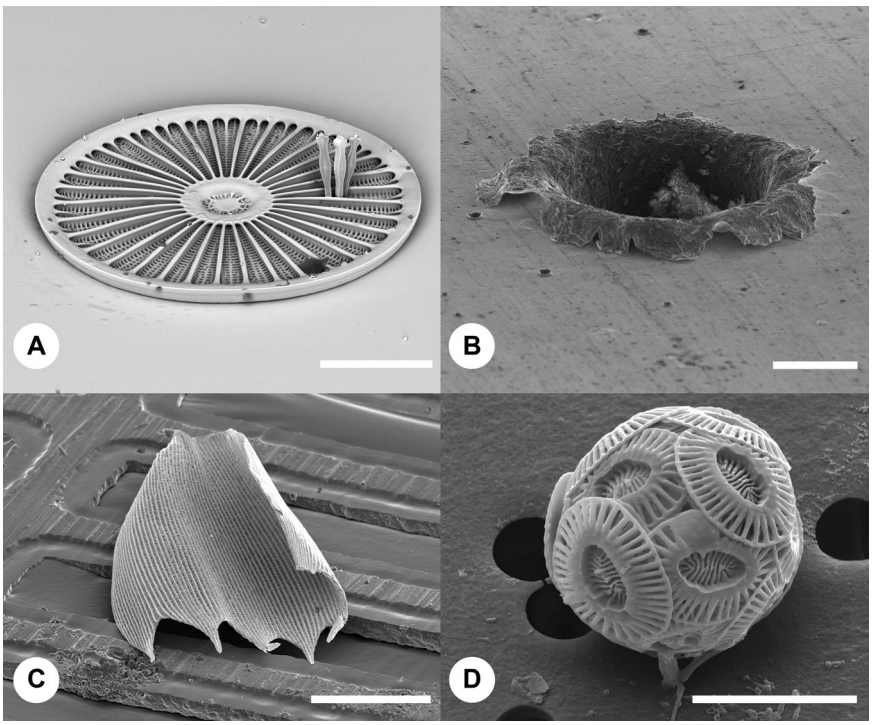

Fig. 6. High-resolution SEM source images, part of the datasets used in the modelling process. (**A**) Diatom with three other diatoms inserted into the frustule to form a miniature 'dartboard', (**B**) simulated micrometeorite hypervelocity impact crater in aluminium foil, (**C**) single isolated butterfly wing scale mounted on a TEM grid and (**D**) coccoliths collected onto a nanopore filter. Scale bars: (**A**) 100 microns, (**B**) 25 microns, (**C**) 100 microns and (**D**) 10 microns.

to reconstruct the scene. Despite an inadequate number of viewpoints, the coccolith model (Fig. 5**D**) compares quite well with its SEM source imagery (Fig. 6**D**). Unfortunately, this specimen (which is around 15 microns in diameter) proved incredibly difficult to keep in the field of view – hence, the paucity of source images. However, these models do prove the feasibility of modelling submicron features by 3D SEM photogrammetry.

Compound eyes appeared to have been captured and modelled effectively, despite being composed of repeating structures (Fig. 2). Unfortunately, these features were not as well reproduced in the 3D meshes used for 3D printing (e.g. compare the models in Fig. 2 to the SEM images in Fig. 4) – the raw datasets were simply too large for 3D printing (they exceeded the maximum file size for the printer) and simplification using standard tools in Meshlab (Quadratic edge collapse) tended to smooth out the surface of the eyes.

3D Printing

The data generated from photogrammetry reconstruction are a hollow mesh and unsuitable for 3D printing. Before it can be printed, the mesh needs to be edited to remove any holes or defects and reduced to a file size suitable for 3D printing. Mesh simplification (polygon reduction) was carried out using Meshlab (http://meshlab.sourceforge.net/). Unfortunately, simplified meshes lose some of the fine-scale details seen in the models. This is a limitation set by the 3D printer used and the computer controlling the printer (a combination of the maximum number of triangles and the total file size). With a higher performance computer and perhaps a different 3D printer, it should be possible to print models with more detail.

Since the initial mesh created is hollow and has no 'thickness', it cannot be 3D printed without increasing the wall thickness to at least 2–3 mm and sealing the edges (Fig. 7**A**). This procedure was carried out using the 'Extrude' function in Autodesk Meshmixer and setting an offset value to determine the wall thickness of the final model. It was also possible to have created the model as a solid, using another Meshmixer tool, but the solid model, while heavier and more robust, used more resin for 3D printing, so the majority of models created were hollow (Figs. 7**B, C**).

3D prints were created using a Formlabs 1+ 3D printer. This desktop SLA printer uses a laser beam to polymerize methacrylate resin slice by slice, extracting the model from the liquid resin reservoir as it prints. The prints could equally have been realized using any other type of 3D printer.

© 2017 The Authors

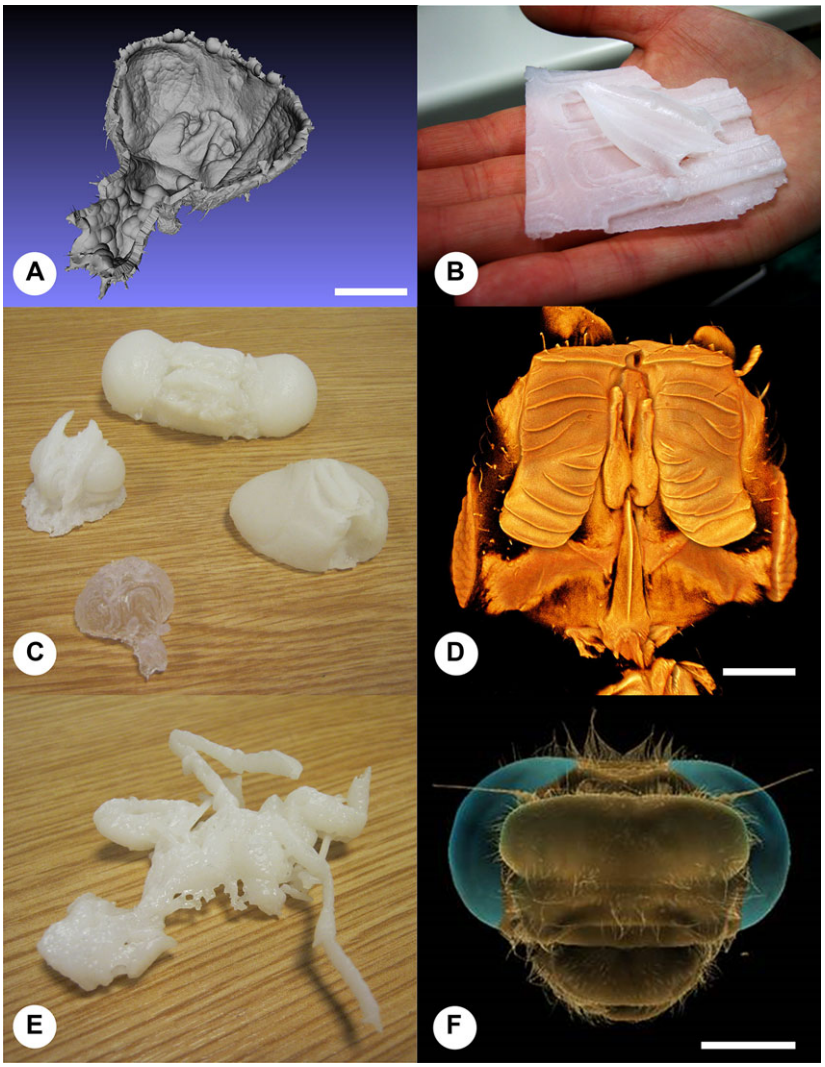

Fig. 7. **(A)** STL mesh in Meshlab, reversed to show thickened back (using Meshmixer) to allow the model to be 3D printed, **(B)** 3D printed butterfly scale showing the level of detail that can be reproduced from the original SEM image data, **(C)** 3D printed models of insect heads, **(D)** confocal microscope 3D model of a fig wasp showing fine detail which can be captured using confocal microscopy, **(E)** 3D print derived from confocal data showing the characteristic stretch along the Z axis caused by the reduced resolution in Z compared to the *X*/*Y* axes and **(F)** 3D model of a dragonfly head derived from micro-CT data, colourized in Drishti. Scale bars: **(A)** 500 μm, **(D)** 100 μm and **(F)** 500 μm.

Discussion

Comparison with confocal microscopy and micro-CT scanning

Confocal microscopy of arthropods, typically through the use of stains to enhance fluorescence (Michels, 2007; Lee *et al.*, 2009; Valdecasas & Abad, 2011; Brooker *et al.*, 2012; Kamanli *et al.*, 2017), is an emerging technique which is proving of great utility for the description of macroinvertebrates. The 3D models, of these specimens, that confocal microscopy yields have good resolution (often submicron) and successfully capture fine-scale structures including setae and fine-scale surface topography which may be only a few hundreds of nanometers in diameter (Fig. 7**D**). However, to reconstruct 3D volumes, this technique requires samples which are fluorescent. If the sample does not fluoresce, then only an upper surface can be captured by reflection confocal microscopy. For example, most terrestrial arthropods have pigmented cuticles which are not fluorescent, none of the insect heads imaged in this study would have been suitable for confocal microscopy. Samples which are too small for light microscopy (e.g. diatoms and butterfly scales) would also be unsuitable for confocal microscopy. It is therefore only suitable when applied to the appropriate subject material. Where the specimens are suitable for confocal microscopy, we have been able to 3D print models. However, the process for converting confocal datasets for

© 2017 The Authors

3D printing is much more time-consuming than for micro-CT or SEM photogrammetry-derived models, in part because confocal datasets frequently contain numerous holes where the data lack signal. Furthermore, the voxels created by confocal microscopy are anisotropic. This is caused by the instruments having considerably lower resolution along the *Z* axis compared to the *X* and *Y* axis. 3D prints created without voxel conversion are 'stretched' along the *Z* axis (Fig. 7**E**). Although confocal data can be converted to isotropic voxels, this does not recover the missing interslice data in the *Z* axis.

Micro-CT scanning of invertebrates comparable to the samples examined in this study has proven to be a highly effective method for collecting high-resolution 3D data. Whether it be through the use of benchtop and laboratory-based micro-CT systems or dedicated synchrotron micro-CT facilities (Betz *et al.*, 2007; Beutel *et al.*, 2008), the results can be extremely impressive. Micro-CT has the additional advantage that the data obtained are composed of isotropic voxels, and segmentation of the data can be used to carry out virtual dissections of the sample to reveal spatial relationships between morphologically important features otherwise hidden within the specimen and therefore only otherwise visible through dissection (Zhang *et al.*, 2010; Wicklein *et al.*, 2012). Micro-CT is most effective in samples which have high contrast compared to the imaging medium (usually air). All of the insect heads studied using the SEM-photogrammetry technique could have been more successfully imaged through laboratory-based micro-CT, although the finest setae would not have been visualized (Fig. 7**F** shows the relatively coarse setation). Samples with very fine-scale features pose challenges for laboratory-based micro-CT systems, with few commercially available instruments currently capable of submicron resolution in 3D. Furthermore, very small samples (<1 mm), which have very low elemental contrast (most nonmineralized biological samples), are extremely challenging to image by micro-CT without the addition of chemical contrast agents (Metscher, 2009; Boyde *et al.*, 2014). The butterfly scale and diatoms imaged in this study for example would prove impossible to image in 3D by micro-CT since they are too small, the features are too fine and the samples themselves would not offer sufficient X-ray attenuation.

Photogrammetry relies on the software being able to match pixels from different images of the same scene taken from different angles. With hard-edged geometric shapes, this is relatively easy, so the technique works well on simple exterior architectural scenes. However, it works less well with repeating regular forms (e.g. brickwork). The most challenging surfaces to model appear to be hair, feathers and other complex, repeating, fine features (Beeler *et al.*, 2012). Conversely, smooth features may offer insufficient opportunities for the software to match points. In the samples we analysed, the software worked best with approximately spherical objects (e.g. the insect heads) and least well for relatively flat objects – especially when those objects were difficult to isolate from the background. Hence, raising the samples above the stub surface using resin beads was more effective than attempting to image samples mounted directly onto stubs. Modelling surfaces with fine texture (setae and scales) was relatively ineffective and this is probably due to the low-resolution image capture systems fitted to the SEMs used in the study. We aim to address this in future studies, using high-resolution image capture systems.

Automation of the image capture process is essential since the process is so time-consuming. However, the accuracy of conventional SEM stages does not appear to be sufficient to provide the repeatable positioning required to consistently centre the sample within the field of view. Using a higher resolution frame store and lower magnification does allow some tolerance in this respect. However, it is clear that to obtain the best results requires the combination of a high-resolution frame store and high precision stage. Correspondence with Stefan Diller (http://www.stefan-diller.com/) suggests that the current generation of encoded piezo stages is capable of maintaining a sample <10 μm in diameter within the centre of the field of view over an extended series of stage moves, and Stefan has demonstrated this for single, isolated cells (http://www.nanoflight.info/nanoflightmovies.html). This stage precision, combined with high-resolution frame stores, opens up the possibility of 3D modelling submicron-scale structures, surfaces and features of low Z-contrast materials at very high-spatial resolution, over larger areas than is currently possible through other techniques using otherwise standard SEMs.

Cheung *et al.* (2013) suggested that high tilt angle rotational SEM might prove a valuable tool for visualizing and sharing complex morphological models. We feel that the present study takes that idea a step further in being able to fully realize the imaging potential of the SEM and in converting its two-dimensional output into 3D models. 3D models of insect heads (blowfly, damselfly, fruit fly and butterfly) produced in this study have been uploaded to Sketchfab (https://sketchfab.com/NHM_Imaging) where they can be viewed and downloaded.

Acknowledgements

PAJ was part-funded through a Royal Microscopical Society Summer Studentship and through the University of Exeter Access to Internships program. PAJ and AELW were also part-funded through an NHM Departmental Investment Fund.

Additional 3D prints for outreach were supplied to us by Richard Woolridge (Technical Specialist) and Nigel Dowsett (Business Manager), created using a Stratasys Objet 1000 3D Resin Printer at Ford Technical Centre, Essex, U.K. David Hubbard at Carl Zeiss Microscopy, UK provided advice and assistance with macro design for the Zeiss microscopes and Remco Geurts at FEI provided us with software to programme the Quanta 650.

© 2017 The Authors

References

Beeler, T., Bickel, B., Noris, G., Beardsley, P., Marschner, S., Sumner, R.W. & Gross, M. (2012) Coupled 3D reconstruction of sparse facial hair and skin. In *ACM Transactions on Graphics (TOG) – Proceedings of ACM SIGGRAPH 2012*. New York, NY. vol. 31(4). Article No. 117.

Betz, O., Wegst, U., Weide, D., Heethoff, M., Helfen, L., Lee, W.K. & Cloetens, P. (2007) Imaging applications of synchrotron X-ray phase-contrast microtomography in biological morphology and biomaterials science. I. General aspects of the technique and its advantages in the analysis of millimetre-sized arthropod structure. *J. Microsc.* **227**, 51–71.

Beutel, R.G., Ge, S. & Hörnschemeyer, T. (2008) On the head morphology of *Tetraphalerus*, the phylogeny of Archostemata and the basal branching events in Coleoptera. *Cladistics* **24**, 270–298.

Boyde, A., Mccorkell, F.A., Taylor, G.K., Bomphrey, R. J. & Doube, M. (2014) Iodine vapor staining for atomic number contrast in backscattered electron and X-ray imaging. *Microsc. Res. Tech.* **77**, 1044–1051.

Brooker, A.J., Shinn, A.P. & Bron, J.E. (2012) Use of laser scanning confocal microscopy for morphological taxonomy and the potential for digital type specimens (e-types). *Aquat. Biol.* **14**, 165–173.

Cheung, D.K-B., Brunke, A.J. Akkari, N., Mara Souza, C. & Pape, T. (2013) Rotational scanning electron micrographs (rSEM): a novel and accessible tool to visualize and communicate complex morphology. *ZooKeys* **328**, 45–57.

Cornille, N., Garcia, D., Sutton, M.A., McNeill, S.R. & Orteu, J.-J. (2003) Automated 3-D reconstruction using a scanning electron microscope. In *SEM Annual Conference & Exposition on Experimental and Applied Mechanics*, Charlotte, NC, June 2–4 2003.

Eulitz, M. & Reiss, G. 2015. 3D reconstruction of SEM images by use of optical photogrammetry software. *J. Struct. Biol.* **191**, 190–196.

Fahlke, J.M. & Autentrieth, M. (2016) Photogrammetry vs. micro-CT scanning for 3D surface generation of a typical vertebrate fossil—a case study. *J. Palaeontol. Techn.* **14**, 1–18.

Falkingham, P.L. (2012) Acquisition of high resolution three-dimensional models using free, open-source, photogrammetric software. *Palaeontologia Electronica* **15**.1.1T.

Kamanli, S.A., Kihara, T., Ball, A.D., Morritt, D. & Clark, P.F. (2017 In press) A 3D imaging and visualisation workflow, utilising confocal microscopy and advanced image processing, using brachyuran crabs (Decapoda: Brachyura: Grapsidae) as test samples. *J. Microsc*. In press. DOI: 10.1111/jmi.12540.

Kearsley, A.T., Graham, G.A., Burchell, M.J., *et al.* (2007) Analytical scanning and transmission electron microscopy of laboratory impacts on Stardust aluminum foils: interpreting impact crater morphology and the composition of impact residues. *Meteorit. Planet. Sci.* **42**, 191–210.

Lee, S., Brown, R.L. & Monroe, W. (2009) Use of confocal laser scanning microscopy in systematics of insects with a comparison of fluorescence from different stains. *Syst. Entomol.* **34**, 10–14.

Mallison, H & Wings, O. (2014) Photogrammetry in paleontology—a practical guide. *J. Palaeontol. Techn*. **12**, 1–31.

Metscher, B.D. (2009) MicroCT for comparative morphology: simple staining methods allow high-contrast 3D imaging of diverse non-mineralized animal tissues. *BMC Physiol*. **9**, 11–25.

Micheletti, N., Chandler, J.H. & Lane, S.N. (2015) Structure from motion (SfM) photogrammetry. Chapter 2, Section 2.2. *Geomorphological Techniques* (Online Edition) (ed. by S. J. Cook, L. E. Clarke & J. M. Nield). British Society for Geomorphology, London, UK. ISSN: 2047–0371.

Michels, J. (2007) Confocal laser scanning microscopy: using cuticular autofluorescence for high resolution morphological imaging in small crustaceans. *J. Microsc*. **227**, 1–7.

Nguyen, C.V., Lovell, D.R., Adcock, M. & La Salle, J. (2014) Capturing natural-colour 3D models of insects for species discovery and diagnostics. *PLoS One* **9**(4), e94346.

Snavely, N., Seitz, S.M. & Szeliski, R. (2008) Modeling the world from Internet photo collections. *Int. J. Comp. Vis.* **80**, 189–210.

Sutton, M. Rahman, I. & Garwood, R. (2014) *Techniques for Virtual Palaeontology*. John Wiley & Sons, Chichester, UK. ISBN: 9781118591130.

Tafti, A.P., Kirkpatrick, A.B., Alavi, Z., Owen, H.A. & Yu, Z. (2015) Recent advances in 3D SEM surface reconstruction. *Micron* **78**, 54–66.

Valdecasas, A.G. & Abad, A. (2011) Morphological confocal microscopy in Arthropods and the enhancement of autofluorescence after proteinase K extraction. *Microsc. Microanal.* **17**, 109–113.

Westoby, M.J., Brasington, J., Glasser, N.F., Hambrey, M.J. & Reynolds, J.M. (2012) 'Structure-from-Motion' photogrammetry: a low-cost, effective tool for geoscience applications. *Geomorphology* **179**, 300–314.

Wicklein, M., Schwyn, D.A., Simonsen, T.J., Howard, L.E., Ball, A.D., Abel, R.L. & Krapp, H.G. (2012). Radiocontrast micro-CT imaging optimised for differential tissue segmentation in *Calliphora vicina* (blowfly). In *Unpublished Poster Abstract Presented at the 15th European Microscopy Congress*. Manchester Central, UK. Available at: http://www.emc2012.org.uk//documents/Abstracts/Abstracts/EMC2012_0874.pdf

Zhang, K., Li, D., Zhu, P., Yuan, Q., Huang, W., Liu, X. & Hong, Y. (2010) 3D visualization of the microstructure of Quedius beesoni Cameron using micro-CT. *Anal. Bioanal. Chem.* **397**, 2143–2148.

© 2017 The Authors